AD-A166 431 CONVECTIVE STABILIZATION OF IONOSPHERIC PLASMA CLOUDS 1/1
(U) NAVAL RESEARCH LAB WASHINGTON DC J F DRAKE ET AL.
19 MAR 86 NRL-MR-5722

UNCLASSIFIED F/G 4/1 NL

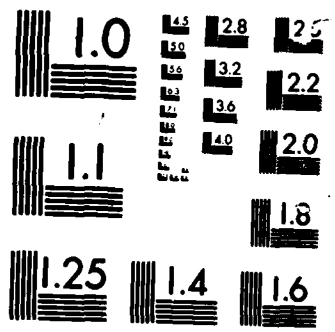

MICROCOPY RESOLUTION TEST CHART

NRL Memorandum Report 5722

Convective Stabilization of Ionospheric Plasma Clouds

J. F. DRAKE

Science Applications International Corporation
McLean, VA 22102
and
University of Maryland
College Park, MD 20742

J. D. HUBA

Geophysical and Plasma Dynamics Branch
Plasma Physics Division

March 19, 1986

This research was sponsored by the Defense Nuclear Agency under Subtask QIEQMXBB, work unit 00005 and work unit title "Plasma Structure Evolution."

NAVAL RESEARCH LABORATORY
Washington, D.C.

SECURITY CLASSIFICATION OF THIS PAGE

REPORT DOCUMENTATION PAGE

1a. REPORT SECURITY CLASSIFICATION UNCLASSIFIED	1b. RESTRICTIVE MARKINGS
2a. SECURITY CLASSIFICATION AUTHORITY	3. DISTRIBUTION/AVAILABILITY OF REPORT Approved for public release; distribution unlimited.
2b. DECLASSIFICATION/DOWNGRADING SCHEDULE	
4. PERFORMING ORGANIZATION REPORT NUMBER(S) NRL Memorandum Report 5722	5. MONITORING ORGANIZATION REPORT NUMBER(S)
6a. NAME OF PERFORMING ORGANIZATION Naval Research Laboratory; 6b. OFFICE SYMBOL *(If applicable)* Code 4780	7a. NAME OF MONITORING ORGANIZATION
6c. ADDRESS *(City, State, and ZIP Code)* Washington, DC 20375-5000	7b. ADDRESS *(City, State, and ZIP Code)*
8a. NAME OF FUNDING/SPONSORING ORGANIZATION Defense Nuclear Agency; 8b. OFFICE SYMBOL *(If applicable)* RAAE	9. PROCUREMENT INSTRUMENT IDENTIFICATION NUMBER
8c. ADDRESS *(City, State, and ZIP Code)* Washington, DC 20305	10. SOURCE OF FUNDING NUMBERS PROGRAM ELEMENT NO. 63223C; PROJECT NO.; TASK NO.; WORK UNIT ACCESSION NO. 47-0889-0-5

11. TITLE *(Include Security Classification)*
Convective Stabilization of Ionospheric Plasma Clouds

12. PERSONAL AUTHOR(S)
Drake, J.F.* and Huba, J.D.

13a. TYPE OF REPORT	13b. TIME COVERED	14. DATE OF REPORT *(Year, Month, Day)*	15. PAGE COUNT
Interim	FROM ____ TO ____	1986 March 19	48

16. SUPPLEMENTARY NOTATION *Science Applications International Corporation, McLean, VA 22102 and University of Maryland, College Park, MD 20742

(Continues)

17. COSATI CODES			18. SUBJECT TERMS *(Continue on reverse if necessary and identify by block number)*
FIELD	GROUP	SUB-GROUP	Plasma clouds; Gradient drift instability; Ionospheric disturbances; Striation freezing

19. ABSTRACT *(Continue on reverse if necessary and identify by block number)*

We derive a stability criteria for the large-scale structuring of ionospheric plasma clouds due to the $E \times B$ gradient drift instability. For the equilibrium we consider a cylindrical 2D waterbag cloud aligned along a uniform magnetic field that is polarized by a neutral wind. We perform a stability analysis that allows three dimensional perturbations (in r, θ, and z), and consider both local and global modes. We find that when the parallel wavenumber k_z exceeds a threshold value, exponentially growing global eigenmodes form which are localized on the "backside" of the cloud. This is in contrast to the $k_z = 0$ limit in which there are no exponential solutions. As k_z is increased further, the unstable modes localize at a finite angle away from the backside; at a point where the diamagnetic propagation velocity (V_d) balances the convective flow velocity of the background plasma around the cloud (V_b). We find that the $E \times B$ gradient drift instability is stable when $V_d > V_b$ so that the cloud is no longer susceptible to large-scale structuring. We apply these results to ionospheric barium clouds and estimate that they will cease structuring when $L_\perp < (cT/eB)(M+2)/2V_n$ where $L_\perp$ is the transverse size of the cloud, $T = T_e + T_i$ is the total temperature, $M = n_c/n_b$,

(Continues)

20. DISTRIBUTION/AVAILABILITY OF ABSTRACT ☒ UNCLASSIFIED/UNLIMITED ☐ SAME AS RPT. ☐ DTIC USERS	21. ABSTRACT SECURITY CLASSIFICATION UNCLASSIFIED
22a. NAME OF RESPONSIBLE INDIVIDUAL J. D. Huba	22b. TELEPHONE *(Include Area Code)* (202) 767-3630; 22c. OFFICE SYMBOL Code 4780

DD FORM 1473, 84 MAR — 83 APR edition may be used until exhausted. All other editions are obsolete.

SECURITY CLASSIFICATION OF THIS PAGE

10. SOURCE OF FUNDING NUMBERS

PROGRAM ELEMENT NO.	PROJECT NO.	TASK NO.	WORK UNIT ACCESSION NO.
DOE		23	DN680-382
61153N		RR011-09-41	DN320-105

CONTENTS

I. INTRODUCTION 1

II. GENERAL EQUATIONS AND EQUILIBRIUM 4

III. LINEARIZED EQUATIONS AND DISPERSION EQUATION 7

IV. EVALUATION OF THE LOCAL DISPERSION EQUATION 11

V. GLOBAL EIGENFUNCTIONS 22

VI. SUMMARY AND CONCLUSION 27

ACKNOWLEDGMENTS 32

REFERENCES 33

CONVECTIVE STABILIZATION OF IONOSPHERIC PLASMA CLOUDS

I. INTRODUCTION

The evolution of artificial plasma clouds (e.g., barium) in the earth's ionosphere continues to be of interest to space plasma physicists after more than two decades of research. The plasma dynamics associated with ionospheric clouds are of interest since they provide a diagnostic of the ambient ionospheric environment, and also provide experimental data for the study of plasma instabilities. Of particular interest is the onset and evolution of the $\underset{\sim}{E} \times \underset{\sim}{B}$ gradient drift instability (Simon, 1963; Hoh, 1963) which is believed to cause the gross structuring of plasma clouds, i.e., field-aligned striations (Linson and Workman, 1970). This instability is also believed to be responsible for, at times, the structuring of the ambient, high latitude F region ionosphere (Keskinen and Ossakow, 1983). The $\underset{\sim}{E} \times \underset{\sim}{B}$ gradient drift instability is an interchange mode and is driven by a neutral wind or dc electric field in an inhomogeneous, weakly collisional plasma. A substantial amount of theoretical and computational research has been carried out to understand the $\underset{\sim}{E} \times \underset{\sim}{B}$ gradient drift instability and its relevance to ionospheric structure (Völk and Haerendel, 1971; Perkins et al., 1973; Zabusky et al., 1973; Shiau and Simon, 1972; Perkins and Doles, 1975; Scannapieco et al., 1976; Chaturvedi and Ossakow, 1979; Keskinen et al., 1980; McDonald et al., 1980, 1981; Huba et al., 1983; Sperling, 1983, 1984; Overman et al., 1983; Sperling and Glassman, 1985; Sperling et al., 1984; Drake et al., 1985).

The bulk of theoretical analyses to date have been based on the local approximation in slab geometry. The local approximation is appropriate for unstable modes which have wavelengths much shorter than the scale length of

Manuscript approved November 19, 1985.

the density gradient associated with the cloud boundary (i.e., $kL \gg 1$ where k is the wavenumber and L is the density gradient scale length) (Huba et al., 1983, Huba and Zalesak, 1983). However, the observed gross structuring of plasma clouds seems to suggest that the dominant modes have $kL \lesssim 1$ so that the local approximation may not be valid. The slab or one-dimensional [$n = n_0(x)$] models of plasma clouds do not include a number of important physical effects which appear in more realistic two-dimensional models. The polarization of large plasma clouds in 2D greatly reduces the relative slip velocity of the cloud and the ambient neutral wind thereby weakening the $\underline{E} \times \underline{B}$ gradient drift instability (Overman et al., 1983; Zalesak and Huba, 1984). Furthermore, convection and/or propagation of the perturbations from the unstable backside to the stable frontside of the cloud may influence the overall stability of 2D models.

The most detailed linear stability analysis of 2D plasma clouds in the long wavelength regime has been based on the waterbag model (Overman et al., 1983). The purpose of this paper is to extend the analysis of Overman et al. (1983) by including parallel dynamics, i.e., density and potential fluctuations along the ambient magnetic field. Recently it has been shown that the parallel effects can strongly influence the linear stability of ionospheric plasma clouds by stabilizing the short wavelength modes (Sperling, 1983; Sperling et al., 1984; Sperling and Glassman, 1985; Drake et al., 1985). However, these investigations have been based on a 1D cloud model and the need to consider a 2D cloud model is apparent. Thus, in this paper we study the influence of parallel dynamics on the stability of 2D ionospheric plasma clouds. In particular, as in Overman et al. (1983) we consider a simple equilibrium consisting of a 2D cylindrical waterbag, but in contrast to them we consider three dimensional perturbations. We find

that the finite parallel dynamics can dramatically alter the $\underline{E} \times \underline{B}$ gradient drift instability. Unlike the limit $k_z = 0$, exponentially growing global eigenmodes can exist when $k_z \neq 0$. As k_z is increased above a threshold value, the unstable modes localize at a finite angle away from the backside; at a point where the diamagnetic propagation velocity (V_d) balances the convective flow velocity of the background plasma around the cloud (V_b). We find that the $\underline{E} \times \underline{B}$ gradient drift instability is stable when $V_d > V_b$ so that the cloud is no longer susceptible to large-scale structuring. We apply these results to ionospheric barium clouds and estimate that they will cease structuring when $L_\perp < (cT/eB)(M+2)/2V_n$ where $L_\perp$ is the transverse size of the cloud, $T = T_e + T_i$ is the total temperature, $M = n_c/n_b$, and n_c is the cloud density, n_b is the background density, and V_n is the neutral wind velocity. For mid-latitude barium releases at ~ 180 km we estimate $L_\perp \sim 160 \rightarrow 480$ m which is consistent with observations.

The organization of the paper is as follows. In the next section we present the assumptions and general equations used in the analysis. In Section III we derive the dispersion equation and in Section IV we present analytical and numerical results. In Section V we investigate the possibility of exponentially growing global eigenmodes. Finally, in Section VI we summarize our findings and discuss the application of our theory to the evolution of ionospheric barium clouds.

II. GENERAL EQUATIONS AND EQUILIBRIUM

The general three dimensional equations for a warm plasma cloud in a uniform magnetic field $\underline{B} = B\,\hat{e}_z$ and a background neutral wind $\underline{V}_n = V_n\,\hat{e}_x$ (see Fig. 1) are given by (Drake et al., 1985)

$$\frac{\partial n}{\partial t} - \frac{c}{B}\nabla\phi \times \hat{z}\cdot\nabla n + \frac{\partial}{\partial z}\frac{1}{e\eta_e}\left(\frac{\partial\phi}{\partial z} - \frac{T_e}{ne}\frac{\partial n}{\partial z}\right) = 0 \tag{1}$$

$$\frac{c}{B}\frac{\nu_{in}}{\Omega_i}\nabla_\perp\cdot n\nabla_\perp\phi + D_{\perp i}\nabla_\perp^2 n + \frac{\nu_{in}}{\Omega_i}\hat{z}\times\underline{V}_n\cdot\nabla n + \frac{\partial}{\partial z}\frac{1}{e\eta_e}\left(\frac{\partial\phi}{\partial z} - \frac{T_e}{ne}\frac{\partial n}{\partial z}\right) = 0 \tag{2}$$

where $\eta_e = m_e\nu_e/ne^2$ is the parallel resistivity, $\nu_e = \nu_{ei} + \nu_{en}$, $D_{\perp i} = (\nu_{in}/\Omega_i)cT_i/eB$ is the perpendicular ion diffusion coefficient, ν_{ei} is the electron-ion collision frequency and Ω_α and $\nu_{\alpha n}$ are the cyclotron and neutral collision frequencies of the species α. Equation (1) is the electron continuity equation and (2) arises from charge neutrality ($\nabla\cdot\underline{J} = 0$). We have considered the electrostatic limit, have assumed ν_e/Ω_e, $\nu_{in}/\Omega_i \ll 1$, and have neglected the ion parallel diffusion $(D_{\parallel i})$ and perpendicular electron diffusion $(D_{\perp e})$. We therefore assume that

$$\partial/\partial t \gg D_{\parallel i}\,\partial^2/\partial z^2,\ D_{\perp e}\,\nabla_\perp^2.$$

It is convenient to change variables by defining a new potential

$$\Phi = \phi + \frac{T_i}{e}\ln(n). \tag{3}$$

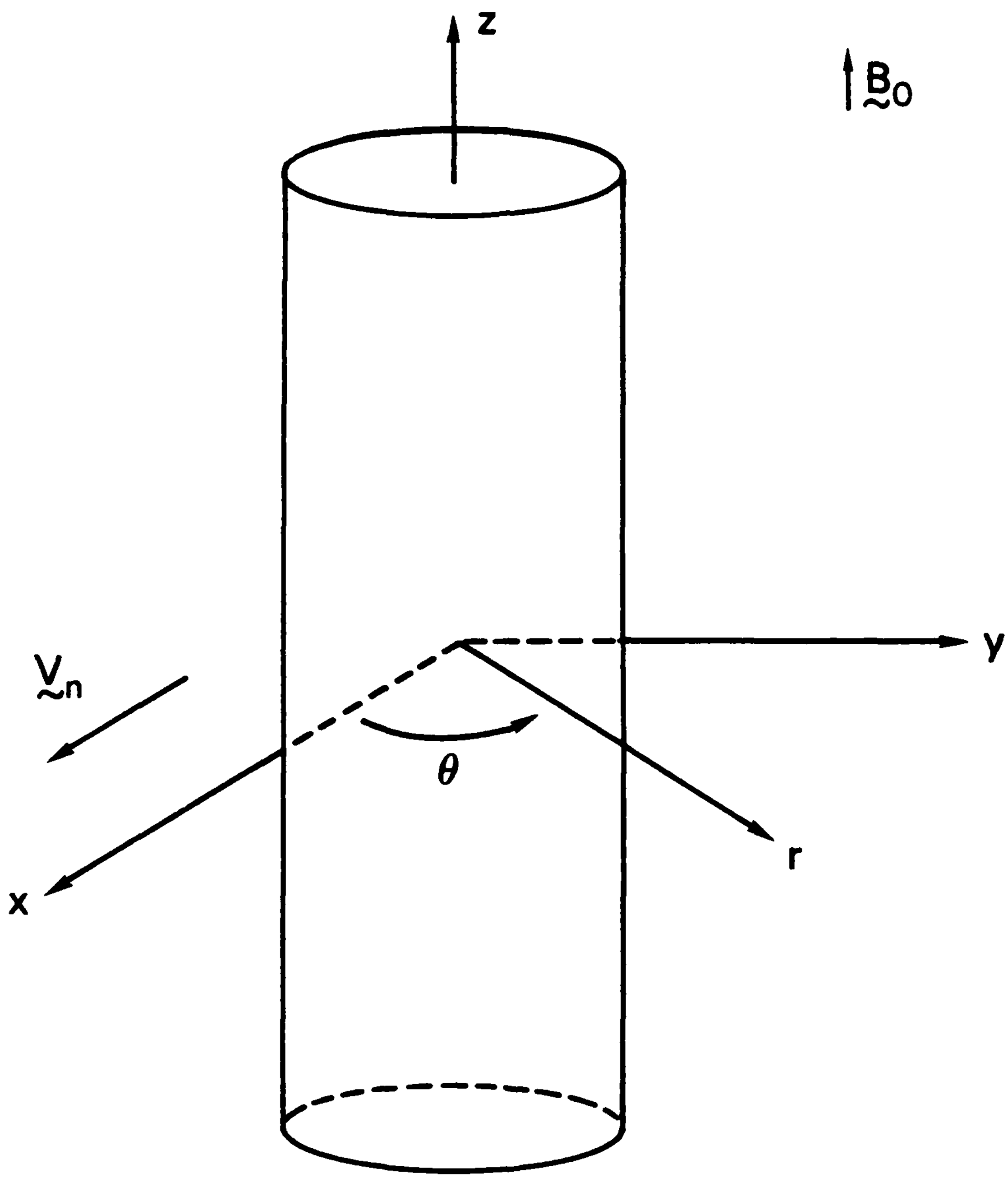

Fig. 1) Cylindrical geometry and plasma configuration used in the analysis.

Equations (1) and (2) then become

$$\frac{\partial n}{\partial t} - \frac{c}{B}\nabla\Phi \times \hat{z}\cdot\nabla n + \frac{\partial}{\partial z}\frac{1}{en_e}\left(\frac{\partial\Phi}{\partial z} - \frac{T}{ne}\frac{\partial n}{\partial z}\right) = 0 \tag{4}$$

$$\frac{c}{B}\frac{\nu_{in}}{\Omega_i}\nabla_\perp\cdot n\,\nabla_\perp\Phi + \frac{\nu_i}{\Omega_i}\hat{z}\times \underline{V}_n\cdot\nabla n + \frac{\partial}{\partial z}\frac{1}{en_e}\left(\frac{\partial\Phi}{\partial z} - \frac{T}{ne}\frac{\partial n}{\partial z}\right) = 0 \tag{5}$$

where $T = T_e + T_i$.

We consider a simple equilibrium consisting of a cylindrical waterbag of radius r_c and density n_c in a uniform background n_b:

$$n_0(r) = n_c H(r_c - r) + n_b \tag{6}$$

where H is the Heaviside function. The solution of the equilibrium equations for this configuration are well known. The drag between the cloud and neutral wind polarizes the cloud. The resulting potential Φ_0 is given by (Smythe, 1950),

$$\frac{c\Phi_0}{B} = \begin{cases} -V_n \dfrac{M}{M+2}\, r\sin\theta & r < r_c \\[2ex] -V_n \dfrac{M}{M+2}\dfrac{r_c^2}{r}\sin\theta & r > r_c \end{cases}$$

where $M = n_c/n_b$. The potential causes the cloud to drift with a uniform velocity

$$\underline{V}_c = V_n \frac{M}{M+2}\hat{e}_x. \tag{7}$$

The linear stability analysis which follows is most easily carried out in the frame of reference of the moving cloud. In this frame the potential Φ_{0c} is given by

$$\frac{c\Phi_{0c}}{B} = \begin{cases} 0 & r < r_c \\ V_n \frac{M}{M+2} \left(r - \frac{r_c^2}{r}\right) \sin\theta . & r > r_c \end{cases} \tag{8}$$

III. LINEARIZED EQUATIONS AND DISPERSION EQUATION.

We investigate the stability of this equilibrium by considering small perturbations $\tilde{n}(r,\theta,z,t)$ and $\tilde{\Phi}(r,\theta,z,t)$ around n_0 and Φ_{0c}. Since the equilibrium is independent of z, we can expand the perturbations in plane waves in the z direction $(\tilde{n}, \tilde{\Phi} \sim \exp ik_z z)$ without loss of generality. In the perpendicular plane such a simple expansion is not generally possible since the equilibrium depends on both r and θ. Equations (4) and (5) yield the linearized equations,

$$\frac{\partial\tilde{n}}{\partial t} - \frac{c}{B} \nabla\Phi_{0c} \times \hat{z}\cdot\nabla\tilde{n} + \frac{c}{B}\frac{n_c}{r_c}\frac{\partial\tilde{\Phi}}{\partial\theta}\delta(r-r_c) - \frac{k_z^2}{en_e}\left(\tilde{\Phi} - \frac{T}{e}\frac{\tilde{n}}{n_0}\right) = 0 \tag{9a}$$

$$\frac{c}{B}\frac{\nu_{in}}{\Omega_i}\left(\nabla_\perp\cdot n_0\nabla\tilde{\Phi} + \nabla_\perp\cdot\tilde{n}\nabla\Phi_{0c}\right) + \frac{\nu_{in}}{\Omega_i}\left(V_n - V_c\right)\frac{\partial\tilde{n}}{\partial y} - \frac{k_z^2}{en_e}\left(\tilde{\Phi} - \frac{T}{e}\frac{\tilde{n}}{n_0}\right) = 0 \tag{9b}$$

Equations (9) are solved separately in the region $r > r_c$ and $r < r_c$, and the solutions are then matched using boundary conditions which are obtained from the equations for $r = r_c$. In the limit $k_z = 0$, this procedure is straightforward since $\tilde{n} = 0$ and $\nabla^2\tilde{\Phi} = 0$ for $r \neq r_c$. In the case $k_z \neq 0$, the equations for $\tilde{n}$ and $\tilde{\Phi}$ in the region $r \neq r_c$ are much more complicated so

further simplifications must be made. We limit the calculation to perturbations for which $\partial/\partial\theta >> 1$. In this limit the θ dependence of $\tilde{n}$ and $\tilde{\Phi}$ can be represented by the eikonal $\tilde{\phi}$, $\tilde{n} \sim \exp[iS(\theta)]$ where

$$\nabla S = ik_\theta(\theta)\,\hat{e}_\theta. \tag{10}$$

In this limit the perturbations are strongly localized around the boundary r_c and decay exponentially away from this boundary. Thus, for $r \neq r_c$ we write

$$\tilde{\phi}_{\pm} = \hat{\phi}_{\pm} \exp[iS(\theta)]\exp[\mp k_{r\pm}(r - r_c)] \tag{11}$$

where + and − refer to the region $r > r_c$ and $r < r_c$, respectively. The specific range of parameters for which the form of $\tilde{\Phi}$ given in (11) is valid will be presented later. Similar expressions can be written for $\tilde{n}_{\pm}(r, \theta)$. Finally, we assume $\tilde{n}$ and $\tilde{\Phi}$ grow exponentially in time with a growth rate γ. For the present, γ must be considered a local growth rate $\gamma(\theta)$. Eventually, we will investigate under what circumstances exponentially growing normal modes of the cloud can exist.

With the form of $\tilde{\Phi}$ (and $\tilde{n}$) given in (11), (9a) and (9b) reduce to algebraic expressions for $k_{r\pm}$ in the regions $r \neq r_c$,

$$k_{r+}^2 - k_\theta^2 - \frac{\alpha_+ k_z^2}{\gamma_+}\Big\{\gamma + ik_\theta \frac{2M}{M+2} V_n \sin\theta$$

$$- \frac{2}{M+2} V_n \frac{\nu_{in}}{\Omega_i}\left[ik_\theta \cos\theta - k_{r+}(1+M)\sin\theta\right]\Big\} = 0 \tag{12a}$$

$$k_{r-}^2 - k_\theta^2 - \frac{\alpha_- k_z^2}{\gamma_-}\Big\{\gamma - \frac{2}{M+2} V_n \frac{\nu_{in}}{\Omega_i}\left[ik_\theta \cos\theta + k_{r-}\sin\theta\right]\Big\} = 0 \tag{12b}$$

$$\gamma_+ = \gamma + k_z^2 D_{\parallel e}^+ + ik_\theta \frac{2M}{M+2} V_n \sin\theta, \tag{12c}$$

$$\gamma_n = \gamma + k_z^2 D_{\parallel e}^n, \tag{12d}$$

$\alpha = \Omega_e\Omega_i/\nu_e\nu_{in} >> 1$, $D_{\parallel e} = T/m_e\nu_e$ is the parallel electron diffusion coefficient and

$$\gamma_\pm \hat{n}_\pm = k_z^2 \hat{\Phi}_\pm/en_{e\pm}. \tag{13}$$

The matching conditions for $\hat{n}_\pm$, $\hat{\Phi}_\pm$ and $k_{r\pm}$ at $r = r_c$ can be derived from (9). The radial $\underline{E} \times \underline{B}$ convection of the cloud causes the density $\tilde{n}$ to be singular at the cloud boundary (third term in the continuity equation). It is convenient therefore to separate out the singular behavior of $\tilde{n}$ so that in the region $r = r_c$

$$\tilde{n}(r, \theta) = [\tilde{N}\ \delta(r-r_c) + \hat{n}_\pm] \exp[iS(\theta)]. \tag{14}$$

The potential $\hat{\Phi}$ remains finite at the boundary so (9a) can be written as

$$[\gamma + k_z^2 D_{\parallel e} + (c/B)\ ik_\theta\ \Phi'_{0c}]\tilde{N} + (c/B)\ ik_\theta n_c\ \tilde{\Phi} = 0. \tag{15}$$

for $r = r_c$. Equation (15) now contains no singularities at $r = r_c$. However, Φ'_{0c} is discontinuous across $r = r_c$ since it is zero for $r < r_c$ and finite for $r > r_c$. The parallel diffusion coefficient $D_{\parallel e}$ is also generally not continuous across the boundary. These discontinuities must be balanced by a corresponding jump in the potential $\tilde{\Phi}$ at the boundary.

Thus, from (8) and (15), we find

$$\hat{\Phi}_+/\gamma_+ = \hat{\Phi}_-/\gamma_- . \tag{16}$$

This condition can also be derived from the requirement that the tangential electric field across the boundary of the plasma cloud be continuous. The continuity equation then reduces to

$$\gamma_- \bar{N} + (c/B) i k_\theta n_c \hat{\Phi}_- = 0. \tag{17}$$

The matching condition for $k_{r\pm}$ can be derived by integrating (9b) across the boundary,

$$- n_b k_{r+} \hat{\Phi}_+ - (n_b + n_c) k_{r-} \hat{\Phi}_- + \frac{B}{c} \frac{2V_n}{M+2} [ik_\theta \cos\theta \, \bar{N} + (1+M) \sin\theta \, \hat{n}_+$$

$$- \sin\theta \, \hat{n}_-] + \frac{(\alpha_+ + \alpha_-)}{2} k_z^2 \frac{T}{e} \bar{N} = 0. \tag{18}$$

Equations (13) and (16)-(18) can then be combined into a single relation between k_{r+} and k_{r-},

$$k_{r+}\gamma_+ + (1+M) k_{r-}\gamma_- - \frac{2V_n}{M+2} [Mk_\theta^2 \cos\theta + (1+M)(\alpha_+ - \alpha_-) \frac{\nu_{in}}{\Omega_i} k_z^2 \sin\theta] \tag{19}$$

$$+ i(\alpha_+ + \alpha_-) \frac{M}{2} k_z^2 k_\theta \frac{cT}{eB} = 0 .$$

Equations (12) and (19) constitute a local dispersion equation for the $\underset{\sim}{E} \times \underset{\sim}{B}$ instability with $k_z \neq 0$ based on a 2D waterbag equilibrium.

IV. EVALUATION OF THE LOCAL DISPERSION EQUATION

We first evaluate the local growth rate $\gamma(\theta)$ by solving the dispersion equation given by (12) and (19). We consider two limits: the cold plasma limit ($T = 0$) and the warm plasma limit ($T \neq 0$).

A. Cold Plasma Limit: $T = 0$

In the cold plasma limit (19) simplifies to

$$k_{r+}\gamma_{+} + (1+M)k_{r-}\gamma_{-} = \frac{2V_n}{M+2}\left[Mk_\theta^2 \cos\theta + (1+M)(\alpha_{+} - \alpha_{-})\frac{\nu_{in}}{\Omega_i}k_z^2 \sin\theta\right] \quad (20a)$$

where

$$\gamma_{+} = \gamma + 2ik_\theta MV_n \sin\theta/(M+2) \quad (20b)$$

$$\gamma_{-} = \gamma \quad (20c)$$

since $D_{\parallel e} \propto T = 0$. Equations (12c) and (12b) for $k_{r\pm}$ remain unchanged. In the limit of small k_z, (12a) and (12b) yield

$$k_{r_\pm} = k_\theta \quad (21a)$$

and the growth rate γ can then be calculated from (20),

$$\gamma = m\gamma_0(\cos\theta - i\sin\theta) \quad (21b)$$

$$\gamma_0 = \frac{2M}{(M+2)^2}\frac{V_n}{r_c} \quad (21c)$$

where $m = k_\theta r_c$ is the poloidal mode number. The growth rate peaks at $\theta = 0$ (the backside of the plasma cloud) and is linearly proportional to m. The growth rate in (21) is consistent with previous rigorous and heuristic investigations of the stability of circular waterbag models of plasma clouds (Overman et al., 1983; Zalesak and Huba, 1984). For $\theta \neq 0$, the second term on the right side of (21b) causes the mode to propagate at a finite frequency. This propagation results as the fluid outside of the cloud convects around the circular boundary and carries the perturbation. The point $\theta = 0$ corresponds to a stagnation point of the flow so there is no finite frequency there. Finally, from (21a) the assumption that the modes are strongly localized around the cloud boundary requires $m \gg 1$.

To obtain analytic expressions for the growth rate of modes with $k_z \neq 0$, we consider only the case $\theta = 0$ which corresponds to the most unstable mode. Later we will present numerical solutions of the more general dispersion relation in which this restriction is relaxed. For simplicity, we also assume that $\nu_e \approx \nu_{en} \gg \nu_{ei}$ so that $\alpha_- \approx \alpha_+ \approx \alpha_b$. For $\theta = 0$, we have $k_{r+} = k_{r-} = k_r$ and $\gamma_+ = \gamma_- = \gamma$ and the dispersion equations are given by,

$$\gamma k_r r_c = m^2 \gamma_0, \tag{22a}$$

$$k_r^2 r_c^2 = m^2 + \lambda^2\left(1 - i\,\frac{M+2}{M}\,\frac{m\gamma_0}{\gamma}\,\frac{\nu_{in}}{\Omega_i}\right) \tag{22b}$$

with the solution

$$\gamma = m\gamma_0\left\{\left[m^2(m^2 + \lambda^2) - \lambda^4\,\frac{(M+2)^2}{4M^2}\,\frac{\nu_{in}^2}{\Omega_i^2}\right]^{1/2} + i\lambda^2\,\frac{M+2}{2M}\,\frac{\nu_{in}}{\Omega_i}\right\}(m^2 + \lambda^2)^{-1} \tag{23a}$$

where

$$\lambda = \alpha_b^{1/2} k_z r_c. \tag{23b}$$

As k_z is increased from zero, over the interval $\lambda < m$ the growth rate is roughly given by its $k_z = 0$ limit. For

$$1 \ll \lambda^2/m^2 \ll \Omega_i^2/\nu_{in}^2 \tag{24a}$$

the growth rate decreases with k_z as

$$\gamma = m^2 \gamma_0/\lambda. \tag{24b}$$

Over this range $k_r = \alpha_b^{1/2} k_z \gg k_\theta$ so that k_z causes the mode to become more localized near the cloud boundary. For

$$\lambda^2 = \alpha_b k_z^2 r_c^2 > \frac{4 M^2}{(M+2)^2} \frac{\Omega_i^2}{\nu_{in}^2} m^2 \tag{25a}$$

the mode is stable. Note that (25a) implies that the lowest order poloidal modes are stabilized first as k_z is increased. The stability condition given in (25b) is only valid for $\nu_{ei} \ll \nu_{en}$. In the opposite limit $\nu_{ei} \gg \nu_{en}$, $\alpha_- = \alpha_b/(1+M)$ and the stability condition can be similarly derived,

$$\lambda^2 = \alpha_b k_z^2 r_c^2 > \frac{4M^2}{[1 + (M+1)^{1/2}]^2} \frac{\Omega_i^2}{\nu_{in}^2} m^2. \tag{25b}$$

To confirm the analytic results for $T = 0$ and to generalize the results for $\theta \neq 0$, we present Figs. 2 and 3 which are obtained by solving (12) and (19) numerically. In each figure we plot (a) the growth rate γ/γ_0 vs. $\lambda = \alpha_b^{1/2} k_z r_c$ and (b) the real frequency ω_r/γ_0 vs. λ for the parameters $m=1$, $\nu_i/\Omega_i = 0.025$, $M = 2$, and $D_{\parallel e} = 0$ (i.e., $T = 0$), and several values of θ: (A) $\theta = 0°$, (B) $\theta = 22.5°$, (C) $\theta = 45°$, (D) $\theta = 67.5°$, and (E) $\theta = 90°$. In Fig. 2 we have taken the limit $\nu_e \simeq \nu_{en} \gg \nu_{ei}$ while in Fig. 3 we consider the opposite limit, $\nu_e \simeq \nu_{ei} \gg \nu_{en}$.

We note the following from Fig. 2 (the limit $\nu_{en} \gg \nu_{ei}$). First, the growth rate γ is a maximum when $k_z = 0$, and decreases as θ increases. For $\theta = 90°$ there is no growth. On the other hand, the real frequency ω_r increases in magnitude as a function of θ for $\lambda = 0$, i.e., $k_z = 0$. These points are consistent with (21). Second, for all values of θ, γ decreases as λ increases which is consistent with (24b), while ω_r remains roughly constant. Finally, the modes become purely propagating for sufficiently large λ, i.e., $\gamma = 0$ but $\omega_r \neq 0$. The value of λ denoted by the arrow in Fig. 2a corresponds to the stabilization point predicted by (25a) which is in excellent agreement with the numerical results. We also note that the stabilization point is independent of θ.

We now discuss Fig. 3 (the limit $\nu_{ei} \gg \nu_{en}$). First, for $\lambda = 0$ we note that γ decreases as θ increases, while ω_r increases in magnitude; this is similar to the results in Fig. 2. Second, in contrast to Fig. 2, we find that a secondary maxima occurs in γ at $\lambda \simeq 36$, and that for finite k_z, modes at $\theta = 90°$ are unstable. This enhanced instability at finite values of k_z is due to the term proportional to $(\alpha_+ - \alpha_-)\sin\theta$ in (20a). For $\nu_{en} \gg \nu_{ei}$ we have $\alpha_+ = \alpha_-$ so that this term does not contribute to the growth of the mode. However, for $\nu_{ei} \gg \nu_{en}$ we note that $\alpha_+ \neq \alpha_-$ so that

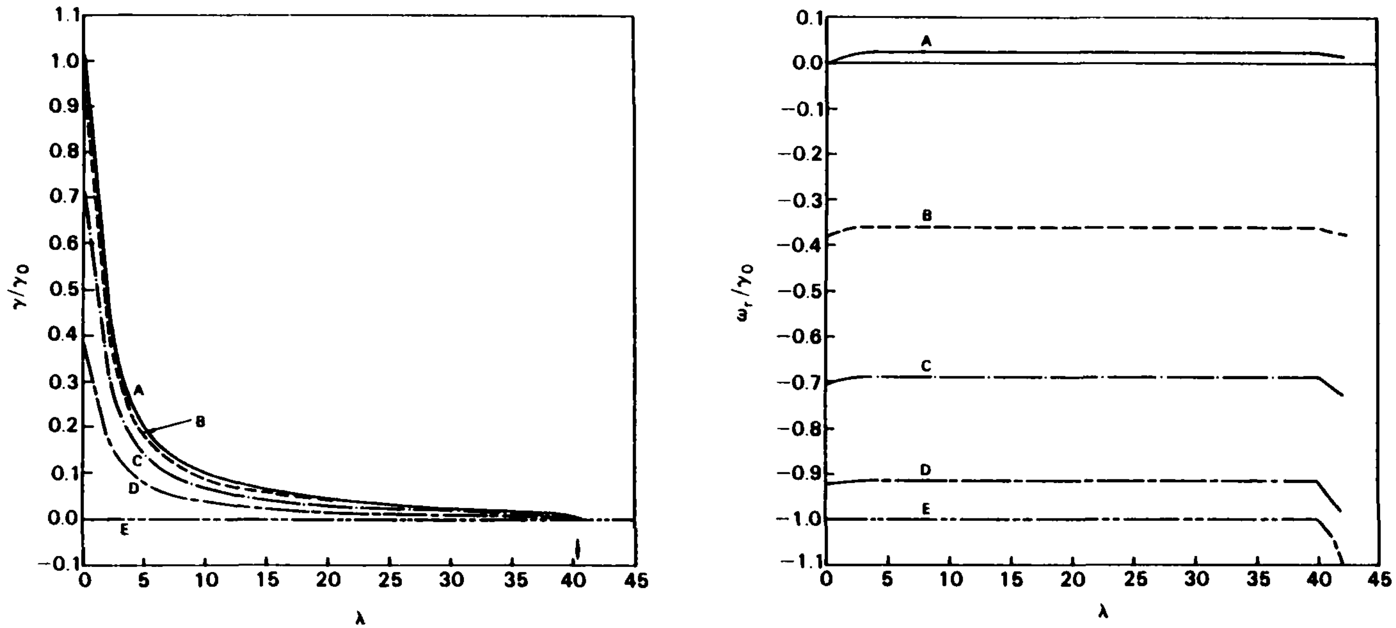

(a) (b)

Fig. 2) Plot of ω/ω_0 vs. $\lambda = \alpha_b^{1/2} k_z r_c$ in the limit $\nu_{en} \gg \nu_{ei}$. The parameters used are m=1, ν_i/Ω_i = 0.025, M=2, $D_{\parallel e}$ = 0 (i.e., T = 0), and several values of θ: (A) θ = 0°, (B) θ = 22.5°, (C) θ = 45°, (D) θ = 67.5°, and (E) θ = 90°. The arrow denotes the value of λ given by (25a) for marginal stability. (a) Plot of the growth rate γ/γ_0 vs. λ. (b) Plot of the real frequency ω_r/γ_0 vs. λ.

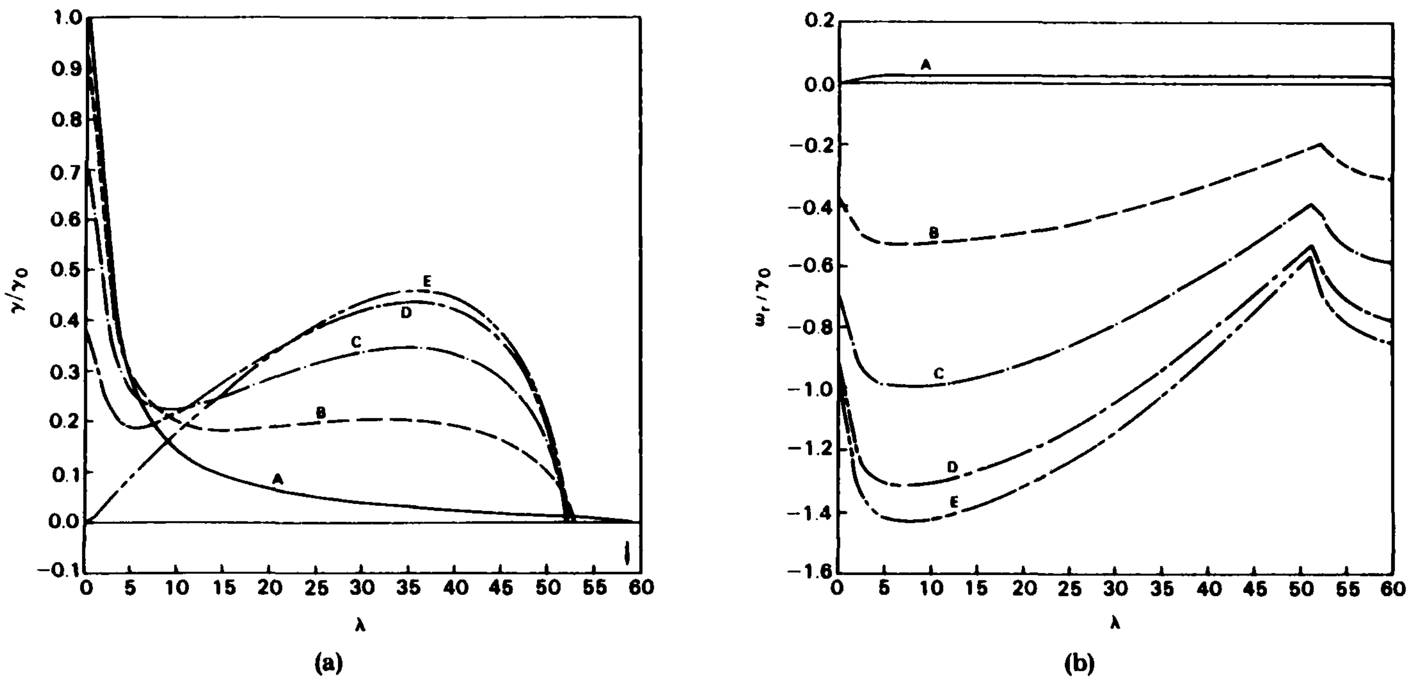

Fig. 3) Plot of ω/ω_0 vs. $\lambda = \alpha_b^{1/2} k_z r_c$ in the limit $\nu_{ei} >> \nu_{en}$. The parameters are the same as in Fig. 2. The arrow denotes the value of λ at marginal stability given by (25b). (a) Plot of the growth rate γ/γ_0 vs. λ. (b) Plot of the real frequency ω_r/γ_0 vs. λ.

this term is finite and positive for $0 < \theta < \pi$. Finally, the modes are stable for sufficiently large λ. The arrow in Fig. 3a denotes the stability condition given in (25b) for $\theta = 0°$; again this value is in excellent agreement with the numerical results.

B. Warm Plasma Limit: $T \neq 0$

We only analytically investigate modes at $\theta = 0$ and again consider the limit $\nu_{en} >> \nu_{ei}$. Equations (12) and (19) reduce to

$$k_r r_c \gamma_{\mp} = m\left(m\gamma_0 \mp i \frac{M}{M+2} \frac{\Omega_i}{\nu_{in}} k_z^2 D_{\parallel e}\right) \tag{26a}$$

$$k_r^2 r_c^2 = m^2 + \lambda^2 \gamma/\gamma_{\mp} \tag{26b}$$

where $k_{r\pm} = k_r$, $\gamma_+ = \gamma_- = \gamma + k_z^2 D_{\parallel e}$ and we have neglected the terms proportional to ν_{in}/Ω_i in (26b) for k_r. This approximation is justified for sufficiently large T (to be proven later).

For $k_z \to 0$, the finite temperature corrections drop out of (26) and the growth rate reduces to $\gamma = m\,\gamma_0$ as in the cold plasma limit. As k_z increases the second term on the right side of (26a) becomes comparable to the driving term γ_0 when $k_z^2 D_{\parallel e} \sim \gamma_0\, \nu_{in}/\Omega_i << \gamma_0$. At this point $k_z^2 D_{\parallel e}$ can still be neglected compared with $\gamma - \gamma_0$ in the definition of γ_-. Thus, the eigenvalue γ is given by

$$\gamma = \frac{(m\gamma_0 - i\omega_0)m}{(m^2 + \lambda^2)^{1/2}}\ , \tag{27a}$$

where

$$k_r^2 r_c^2 = m^2 + \lambda^2 \tag{27b}$$

$$\omega_0 = \frac{M}{M+2}\,\frac{cT}{eB}\,\frac{\lambda^2}{r_c^2} \tag{27c}$$

Thus, k_z decreases the growth rate as in the $T = 0$ limit and causes the mode to propagate at a finite frequency which increases with k_z.

When $k_z^2 D_{\parallel e} \gg \gamma_0 \nu_{in}/\Omega_i$, the modes to lowest order simply propagate at the frequency given in (27a). To calculate the growth rate in this limit, $k_z^2 D_{\parallel e}$ can no longer be neglected compared with γ in γ_-. In (26b) we assume $k_z^2 D_{\parallel e} \ll \gamma$ so that

$$k_r r_c = (m^2 + \lambda^2)^{1/2} - \frac{\lambda^2}{(m^2 + \lambda^2)^{1/2}}\,\frac{k_z^2 D_{\parallel e}}{2\gamma}$$

and from (26a)

$$\gamma = \left(- i\omega_0 + m\gamma_0\right) \frac{m}{\left(m^2 + \lambda^2\right)^{1/2}} - k_z^2 D_{\parallel e}\,\frac{m^2 + \lambda^2/2}{\left(m^2 + \lambda^2\right)} \,. \tag{28a}$$

The $\underline{E} \times \underline{B}$ gradient drift instability is stable for

$$k_z^2 D_{\parallel e}\,\frac{m^2 + \lambda^2/2}{\left(m^2 + \lambda^2\right)^{1/2}} > m^2\gamma_0. \tag{28b}$$

Note that this inequality again implies that the lowest poloidal mode numbers are stabilized first. The assumption that $\gamma \gg k_z^2 D_{\parallel e}$ is valid at the stability point for

$$k_\theta \rho_i \gg \left(V_n/v_i\right)\nu_{in}^2/\Omega_i^2. \tag{28c}$$

Also, the neglect of the terms proportional to ν_{in}/Ω_i in (12a) and (12b) near the stability point are valid in this same limit. Thus, when (28c) is

satisfied, finite temperature effects stabilize the $\underset{\sim}{E} \times \underset{\sim}{B}$ instability, and the stability point is given in (28b). In the opposite limit

$$k_\theta \rho_i \ll (V_n/v_i)\, \nu_{in}^2/\Omega_i^2, \tag{29}$$

the cold plasma effects stabilize the mode and the stability point is given in (25). An expression similar to that given in (28b) can again be derived in the limit $\nu_{ei} \gg \nu_{en}$.

To verify our analytic results for $T \neq 0$, and to extend these results to $\theta \neq 0$, as well as to both $\nu_{en} \gg \nu_{ei}$ and $\nu_{ei} \gg \nu_{en}$, we present numerical solutions to the complete dispersion equation [(12) and (19)]. In Figs. 4 and 5 we plot (a) the growth rate γ vs. λ, and (b) the real frequency ω_r vs. λ for the parameters $m=1$, $\nu_i/\Omega_i = 0.025$, $M = 2$, $D^b_{\parallel e}/\alpha_b r_c^2 \gamma_0 = 5.0 \times 10^{-4}$, and several values of θ: (A) $\theta = 0°$, (B) $\theta = 22.5°$, (C) $\theta = 45°$, (D) $\theta = 67.5°$, and (E) $\theta = 90°$. In Fig. we 4 consider the limit $\nu_e = \nu_{en} \gg \nu_{ei}$, while in Fig. 5 we take $\nu_e = \nu_{ei} \gg \nu_{en}$. Thus, Fig. 4 corresponds to the warm temperature limit of Fig. 2 and Fig. 5 corresponds to that of Fig. 3.

In Fig. 4 we note several similarities to Fig. 2. The growth rate γ decreases as θ or k_z increases and the mode is stable ($\gamma < 0$) for sufficiently large k_z. On the other hand, for $T \neq 0$ (or $D_{\parallel e} \neq 0$) the mode stabilizes at a much smaller value of k_z (other parameters being equal) and the stability point is sensitive to θ. The arrow denotes the value of λ for marginal stability ($\gamma = 0$) based on (28b) for $\theta = 0°$. This value ($\lambda = 15.8$) is in very good agreement with the numerical results ($\lambda = 15.5$).

In Fig. 5 there are also similarities to Fig. 3. For $k_z = 0$, the growth rate γ decreases and the real frequency ω_r increases in magnitude

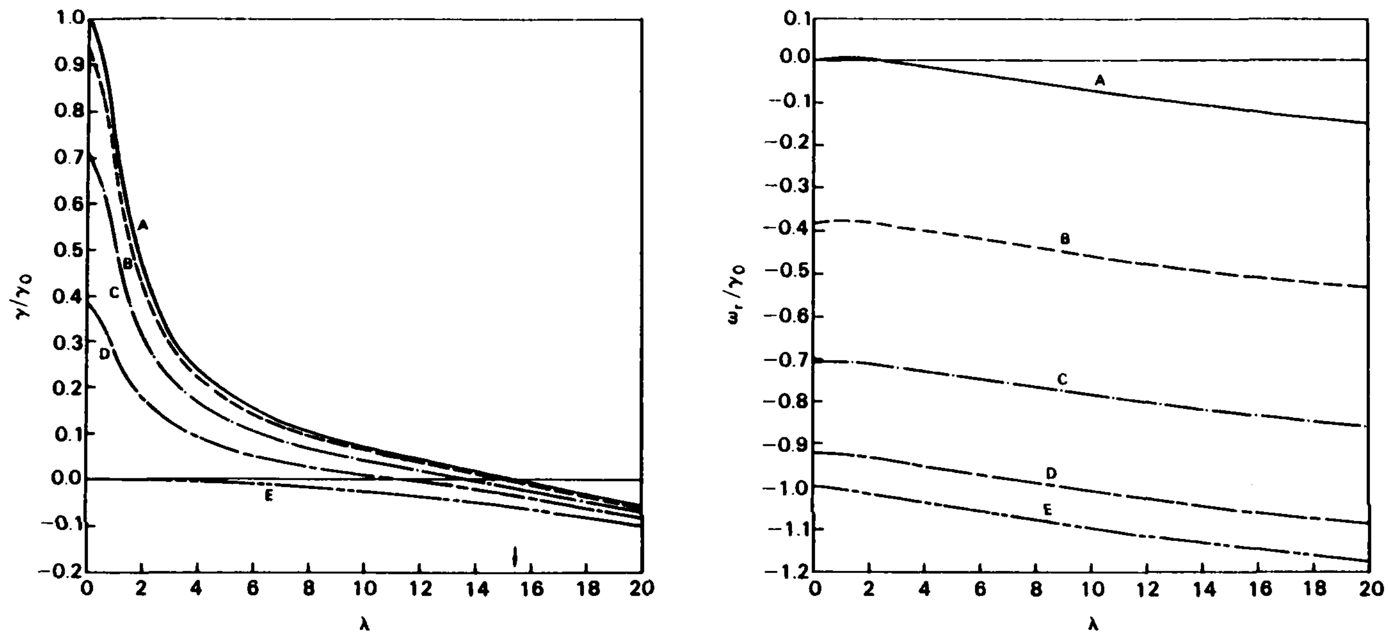

(a) (b)

Fig. 4) Plot of ω/Υ_0 vs. $\lambda = \alpha_b^{1/2} k_z r_c$ in the limit $\nu_{en} >> \nu_{ei}$. The parameters are the same as in Fig. 2 except we assume $T \neq 0$ and take $D_{\parallel e}^{b}/\alpha_b r_c^2 \Upsilon_0 = 5.0 \times 10^{-4}$. (a) Plot of the growth rate Υ/Υ_0 vs. λ. (b) Plot of the real frequency ω_r/Υ_0 vs. λ.

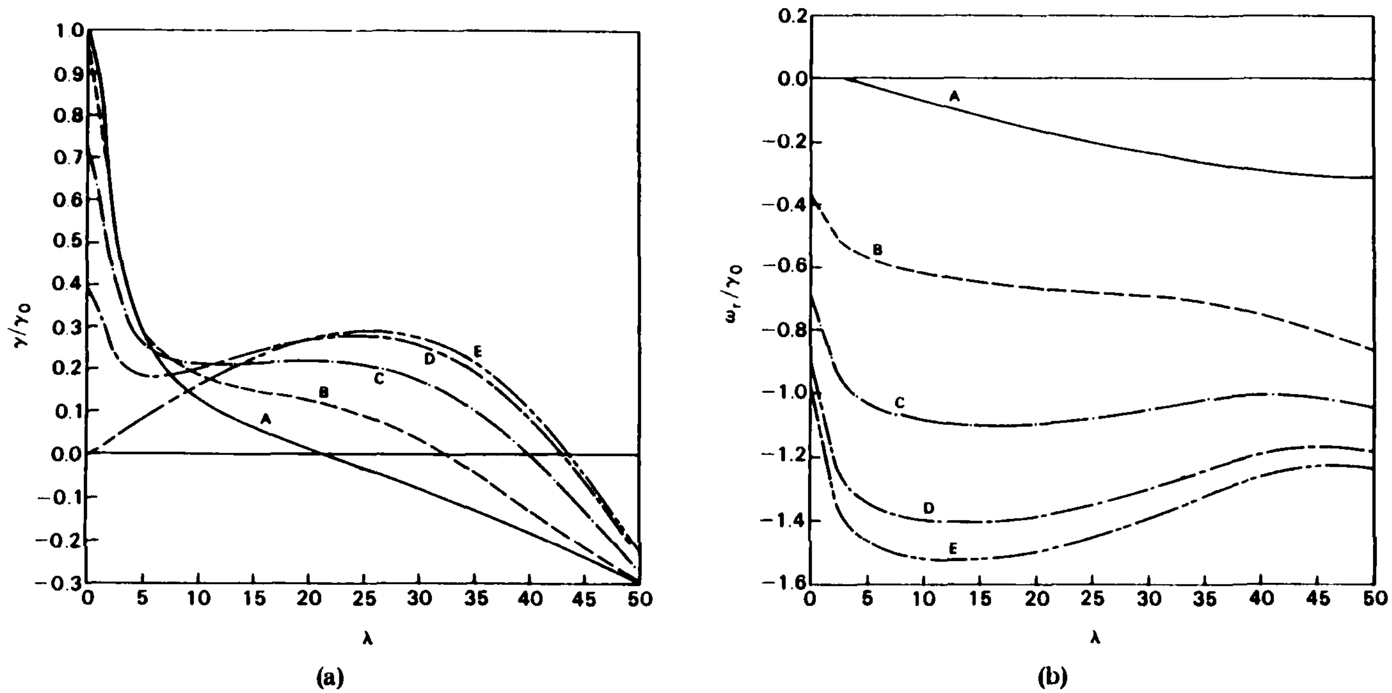

Fig. 5) Plot of ω/ω_0 vs. $\lambda = \alpha_b^{1/2} k_z r_c$ in the limit $\nu_{ei} \gg \nu_{en}$. The parameters are the same as in Fig. 4.

as θ increases. A secondary maxima (or plateau) in γ occurs for a finite value of k_z. However, in contrast to Fig. 2, the value of k_z at marginal stability increases with θ so that the most difficult mode to stabilize is at $\theta = 90°$. Also, the value of k_z at marginal stability is smaller than when $T = 0$.

It is also illuminating to calculate the damping rate of the instability in the limit of very large k_z. There are two modes of the system. The first damps at the ion diffusion rate,

$$\gamma = - |k_r|^2 D_\perp \tag{30a}$$

where

$$k_r = -i\, k_\theta \frac{\Omega_i}{\nu_{in}} \frac{M}{M+2} \tag{30b}$$

and $D_\perp = (cT/eB)\nu_{in}/\Omega_i$ is the ion diffusion coefficient based on the total temperature $T = T_e + T_i$. The second damps at the electron parallel diffusion rate

$$\gamma = - k_z^2\, D_{\parallel e}. \tag{31}$$

V. GLOBAL EIGENFUNCTIONS

In Section III we derived a local dispersion equation [(12) and (19)] which was solved to obtain the growth rate $\gamma(\theta)$ in Section IV. This local growth rate is peaked on the backside of the cloud ($\theta = 0$). We now investigate under what conditions the gradient drift instability forms a global eigenmode as it grows on the cylindrical waterbag.

Such global eigenmodes can exist if solutions $\bar{\phi}(\theta)$ can be constructed which are localized around some angle θ_0. To obtain these solutions we take the growth rate in (12) and (19) to be independent of θ so that the dispersion equation yields $k_\theta(\theta,\gamma)$. We then make the identification $k_\theta = -i\, r_c^{-1}\, \partial/\partial\theta$ to obtain a differental equation for $\bar{\phi}(\theta)$.

In the limit $\lambda^2 = \alpha\, k_z^2 r_c^2 \ll 1$, (12) yields $k_{r\pm} = k_\theta$ and the local dispersion equation in (19) becomes

$$\gamma_0\, \partial\bar{\phi}/\partial\theta - i\gamma\, \exp(i\theta)\bar{\phi} + \omega_0\bar{\phi} = 0. \qquad (32)$$

Since this equation is first order in $\partial/\partial\theta$, there are no bounded solutions so that there are no exponentially growing global eigenmodes when k_z is small. This result is consistent with previous calculations in the limit $k_z = 0$ where it was shown that the energy always cascades to lower poloidal mode numbers (Overman et al., 1983). The local growth rate [see (11)] is the approximate rate of increase of the amplitude of a broad spectrum of modes centered around k_θ.

We now consider the case where $\lambda^2 \gg 1$ while k_z is sufficiently small so that the terms proportional to ν_{in}/Ω_i in (12a) and (12b) can be neglected. We also assume that $\gamma \gg k_z^2 D_{\parallel e}$ and $\nu_{en} \gg \nu_{ei}$. With these constraints (12a) and (12b) simplify to

$$k_{r\pm} = \alpha^{1/2} k_z$$

and (19) yields the equation

$$\gamma_0 \cos\theta \frac{\partial^2}{\partial\theta^2}\bar{\phi} + [\omega_0 + \gamma_0\, \lambda\, \sin\theta]\frac{\partial}{\partial\theta}\bar{\phi} + \gamma\, \lambda\bar{\phi} = 0. \qquad (33)$$

We simplify this equation by defining a new dependent variable

$$\tilde{\phi} = \hat{\phi} \exp[-f(\theta)]$$

with $\partial f/\partial\theta = [\omega_0 + \gamma_0 \lambda \sin\theta]/2\gamma_0 \cos\theta$ and find that

$$\partial^2\hat{\phi}/\partial\theta^2 + V(\theta)\hat{\phi} = 0 \tag{34a}$$

where the potential $V(\theta)$ is given by

$$V(\theta) = \{(\frac{\gamma}{\gamma_0} \cos\theta - \frac{1}{2}) \lambda - \frac{\omega_0}{2\gamma_0} \sin\theta$$

$$- \frac{1}{4\gamma_0^2} [\omega_0 + \gamma_0 \lambda \sin\theta]^2\} \frac{1}{\cos^2\theta} . \tag{34b}$$

We first consider the limit $T = 0$ and expand $V(\theta)$ around $\theta = 0$,

$$V = \lambda(\frac{\gamma}{\gamma_0} - \frac{1}{2}) - \frac{1}{4} \lambda^2\theta^2. \tag{35}$$

The bound state solutions for this potential have eigenvalues

$$\gamma = \gamma_0(n+1), \tag{36}$$

where n is a non-negative integer. The mode is localized on the backside of the cloud and has an angular width $\Delta\theta \sim \lambda^{-1/2} << 1$, which decreases with increasing k_z. Thus, the expansion of V around $\theta = 0$ is valid for $\lambda >> 1$. Note also that higher order modes n, which have more structure in the

poloidal direction, have larger growth rates. This result is consistent with local theory where γ increases with the poloidal mode number m.

The potential V in (34) is modified by finite thermal effects when $\omega_0 \sim \gamma_0\lambda$. Comparing the magnitude of the various terms in (34), we find that the term proportional to $(4\gamma_0^2)^{-1}$ is of order $\lambda \gg 1$ larger than the remaining terms unless the terms within the bracket cancel. We therefore look for a mode localized around the angle θ_0 defined by

$$\sin\theta_0 = -\omega_0/\gamma_0\lambda. \tag{37}$$

Near θ_0 the potential assumes the form

$$V(\theta) = \lambda \frac{\gamma}{\gamma_0} \frac{1}{\cos\theta_0} - \frac{1}{2}\lambda - \frac{1}{4}\lambda^2(\theta - \theta_0)^2. \tag{38}$$

The bounded solutions have eigenvalues

$$\gamma = \gamma_0(n+1)\left[1 - \frac{\omega_0^2}{\gamma_0^2\lambda^2}\right]^{1/2}, \tag{39}$$

where n is again a non-negative integer. When $\omega_0 \ll \gamma_0\lambda$, the growth reduces to the previous zero temperature result in (36). As ω_0 increases the growth rate decreases until the mode becomes stable at $\omega_0 = \gamma_0\lambda$ or

$$\alpha^{1/2} k_z \frac{cT}{eB} > \frac{2}{M+2} V_n . \tag{40}$$

The reduction of the growth rate in (39) is a consequence of the localization of the mode at an angle $\theta_0 \neq 0$. The growth rate in (39) can be rewritten as

$$\gamma = \gamma_0(n+1)\cos\theta_0.$$

At the marginal stability point, $\theta_0 = \pi/2$, i.e., the mode localizes in a region where there is no driving force. Above the threshold in (40) there are no bounded solutions to (34) since θ_0 moves into the complex plane.

The physics behind the localization of the mode can be readily understood. As we discussed previously in Sec. IV, the convection of the background plasma past the cloud causes the mode to propagate with a frequency [see (21b)]

$$\omega_r = m\gamma_0 \sin\theta. \tag{41}$$

On the other hand, the thermal effects cause the mode to propagate with a frequency [see (27a)]

$$\omega_r = m\omega_0/\lambda. \tag{42}$$

These two frequencies balance each other at the angle θ_0 given in (37). The mode localized at this angle has no real frequency and grows at the local growth rate corresponding to this angle. When the propagation rate due to the thermal effects is everywhere larger than the convection flow no localized solutions exist. In this regime the $\underline{E} \times \underline{B}$ gradient drift instability is effectively stable since, unlike the limit where $k_z = 0$, the rate of propagation of the mode from the unstable backside of the cloud to the stable frontside exceeds the rate of growth of the mode. Convective amplification of perturbations in this finite k_z limit is therefore not significant.

VI. SUMMARY AND CONCLUSION

We have investigated the influence of finite parallel wavelength on the stability of a cylindrical plasma cloud. We first derived a dispersion relation for the local growth rate $\gamma(\theta)$ of the $\underset{\sim}{E} \times \underset{\sim}{B}$ gradient drift instability, where θ is the poloidal angle ($\theta = 0$ on the "backside" of the cloud as shown in Fig. 1). For sufficiently large values of the parallel wavenumber k_z the local growth rate is negative for all values of θ. In the cold plasma limit,

$$k_\theta \rho_i < (V_n/v_i)\nu_{in}^2/\Omega_i^2 \qquad (43)$$

the stability criterion is given in (25a) while in the warm plasma limit [the inequality in (43) is reversed], the stability condition is given in (28b). In both cases the lowest poloidal mode numbers are stabilized at the smallest values of k_z.

We have also investigated under what conditions exponentially growing global eigenmodes can exist. In the limit

$$\lambda^2 = \alpha k_z^2 r_c^2 \ll 1 \qquad (44)$$

with $\alpha = \Omega_e \Omega_i/\nu_e \nu_{in}$ there are no exponentially growing solutions. In this limit the energy cascades to lower poloidal mode numbers as the instability grows as found by Overman et al. (1983). When $\lambda^2 \gg 1$ a localized mode of angular width $\theta \sim \lambda^{-1/2} \ll 1$ forms on the "backside" of the plasma cloud and grows exponentially in time. Thus, the cascade of energy to lower mode numbers no longer takes place when k_z is sufficiently large. The structure of the mode for this case is illustrated in Fig. 6a. This figure is drawn

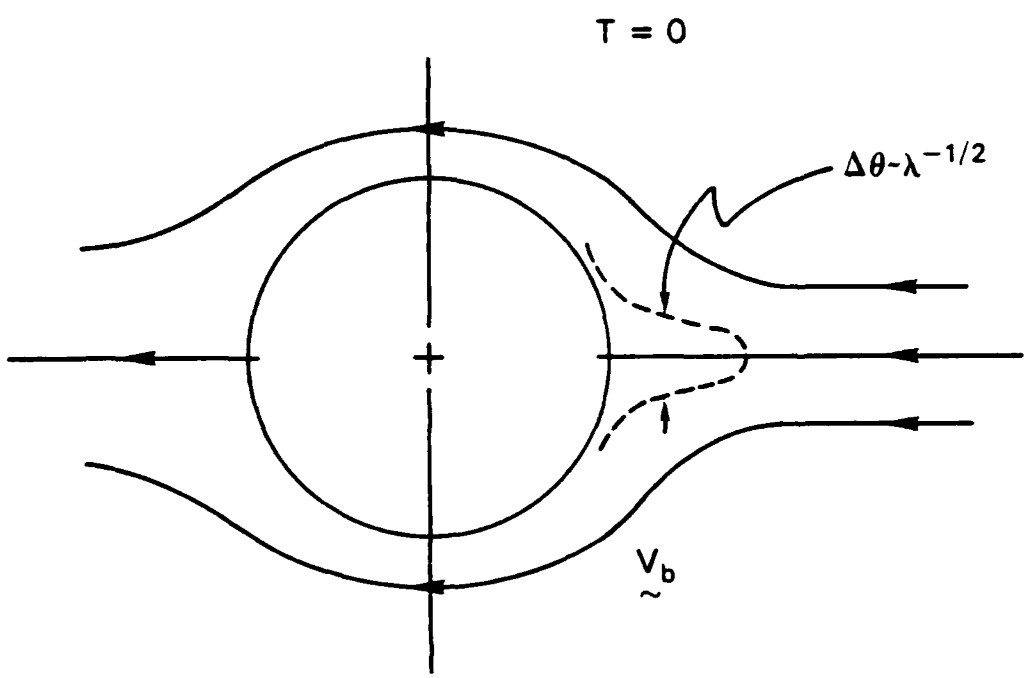

(a)

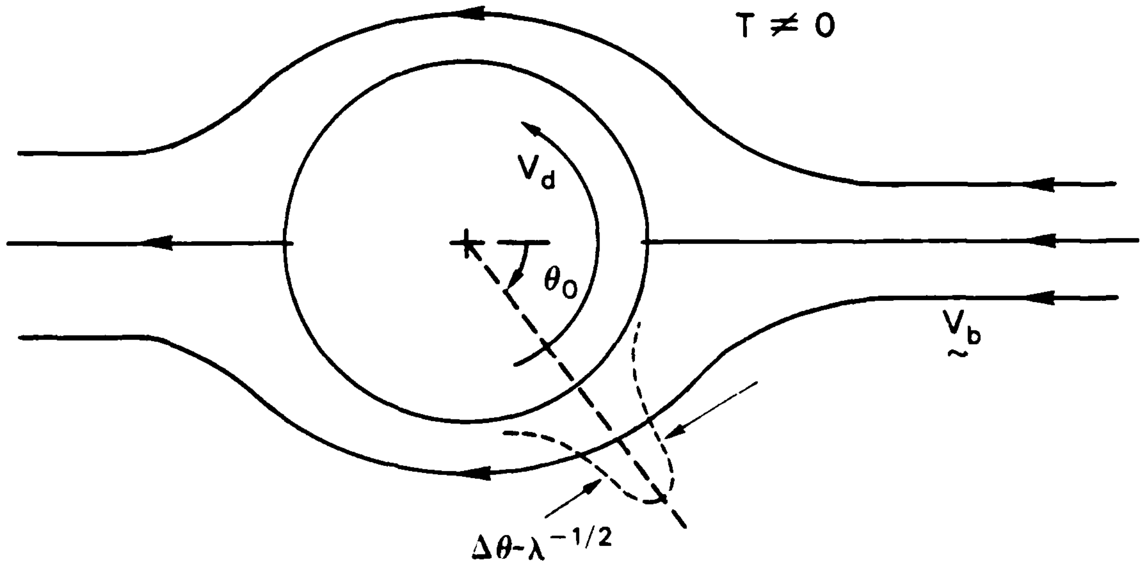

(b)

Fig. 6) Schematic of the plasma cloud, flow field, and position of a growing eigenfunction: (a) T = 0; (b) T ≠ 0. See text for a detailed description.

in the rest frame of the circular cloud. The neutral wind is moving from the left to right with a uniform velocity $2V_n/(M+2)$ while the background plasma flows to the left with a velocity $\underline{V}_b$. The dashed line illustrates the amplitude of the lowest order mode. At still larger values of k_z the unstable mode becomes localized at a finite angle θ_0 given by

$$\sin\theta_0 = - V_d/V_b \tag{45}$$

where

$$V_d = M \frac{cT}{eB} \alpha^{1/2} k_z$$

is the effective diamagnetic velocity and

$$V_b = \frac{2M}{M+2} V_n$$

with $M = n_c/n_b$. For a waterbag distribution the density scale length which usually appears in definition of the diamagnetic drift velocity is replaced by the radial scale length, $\alpha^{-1/2} k_z^{-1}$. For $V_d > V_b$ or

$$\alpha^{1/2} k_z \frac{cT}{eB} > \frac{2}{M+2} V_n \tag{46}$$

the mode is completely stable. The physical mechanism which causes the localization at θ_0 as well as the stabilization is illustrated in Fig. 6b. In the local dispersion relation the diamagnetic effects cause the mode to propagate in the poloidal direction with a frequency

$$\omega = k_\theta V_d/(M+2),$$

where k_θ is the poloidal wavenumber. The velocity of the background plasma just outside the cloud (in the reference frame of the cloud) is given by

$$\underline{V} = V_b \sin\theta \, \hat{\theta}.$$

The convection of the background plasma past the cloud causes the mode to propagate with a frequency

$$\omega = k_\theta V_b \sin\theta.$$

These two frequencies balance to produce a non-propagating mode at the angle θ_0 defined in (45). The dashed line in Fig. 6b illustrates the localization of the mode in this case. When the diamagnetic velocity everywhere exceeds the flow of the background plasma around the cloud the gradient drift instability is convectively stabilized.

Finally, we apply these results to the structuring of barium clouds and discuss their application to the so-called "striation freezing" phenomenon (Linson and Meltz, 1972). Basically, it has been observed that barium clouds released in the ionosphere structure because of the $\underline{E} \times \underline{B}$ gradient drift instability and develop field-aligned striations. The first generation of striations can also undergo further structuring, at times, and break up into even smaller striations (i.e., smaller in size transverse to $\underline{B}_0$). This process, known as bifurcation, appears to continue until a minimum transverse scale size is reached (which we refer to as the "freezing scale length"). For barium clouds released at altitudes ~ 180 km the freezing scale length is roughly 400 m (Prettie, 1985). A number of

studies have been carried out which address this problem (Francis and Perkins, 1975; McDonald et al., 1981; Zalesak et al., 1984; Drake et al., 1985; Sperling and Glassman, 1985). Rather than describe the detailed processes proposed in these papers, it is sufficient to note that there is no generally accepted model of striation freezing at this time; each model has its merits and shortcomings. Although the theory presented in this paper does not explicitly predict a "freezing scale length", we can make an estimate of this size based on (46) and a simple physical argument. The free parameter in (46) is k_z; all other parameters are determined by ionospheric conditions. Thus, we need to make a reasonable estimate of k_z. We do this by noting that transverse perturbations can map parallel to the magnetic field. The relationship between parallel and perpendicular scale lengths is approximately given by $L_\parallel \sim (\sigma_\parallel/\sigma_\perp)^{1/2} L_\perp = \alpha^{1/2} L_\perp$ where L and σ refer to the scale size and conductivity, respectively (Farley, 1959; Goldman et al., 1976). Assuming that $k_z \sim L_\parallel^{-1} \sim (\alpha^{1/2} L_\perp)^{-1}$ we find that (46) can be written as

$$L_\perp < \frac{M+2}{2} \frac{cT}{eB} \frac{1}{V_n} . \qquad (47)$$

Thus, (47) suggests that barium cloud striations with transverse dimensions smaller than $L_\perp$ would be stable to further structuring by the $\underset{\sim}{E} \times \underset{\sim}{B}$ gradient drift instability. For typical barium cloud ionospheric parameters at 180 km, i.e., $T = T_e + T_i \sim 0.2$ eV, $B \sim 0.5$ G, $V_n \sim 50$ m/sec, and $M \sim 2$-10, we find that $L_\perp \sim 160$-480 m which is consistent with observations. Of course this result is predicated on the assumption that $k_z \sim (\alpha^{1/2} L_\perp)^{-1}$ which, although plausible, is somewhat ad hoc. In order to remove this assumption it is necessary to consider the finite length of a barium cloud

which introduces a physical parameter which will remove the arbitrariness associated with k_z. We are presently developing such a model.

ACKNOWLEDGMENTS

We thank Steve Zalesak and Norm Zabusky for helpful discussions. This research has been supported by the Defense Nuclear Agency.

REFERENCES

Chaturvedi, P.K., and S.L. Ossakow, Nonlinear stabilization of the E × B gradient drift instability in ionospheric plasma clouds, J. Geophys. Res., 84, 419, 1979.

Drake, J.F., J.D. Huba, and S.T. Zalesak, Finite temperature stabilization of the gradient drift instability in barium clouds, J. Geophys. Res., 90, 5227, 1985.

Farley, D.T., Jr., A theory of electrostatic fields in a horizontally stratified ionosphere subject to a vertical magnetic field, J. Geophys. Res., 64, 1225, 1959.

Francis, S.H., and F.W. Perkins, Determination of striation scale sizes for plasma clouds in the ionosphere, J. Geophys. Res., 80, 3111, 1975.

Goldman, S.R., L. Baker, S.L. Ossakow, and A.J. Scannapieco, Striation formation associated with barium clouds in an inhomogeneous ionosphere, J. Geophys. Res., 81, 5097, 1976.

Hoh, F.C., Instability of Penning-type discharges, Phys. Fluids, 6, 1184, 1963.

Huba, J.D., S.L. Ossakow, P. Satyanarayana, and P.N. Guzdar, Linear theory of the E × B instability with an inhomogeneous electric field, J. Geophys. Res., 88, 425, 1983.

Huba, J.D., and S.T. Zalesak, Long wavelength limit of the E × B instability, J. Geophys. Res., 88, 10,263, 1983.

Keskinen, M.J., S.L. Ossakow, and P.K. Chaturvedi, Preliminary report of numerical simulations of intermediate wavelength E × B gradient drift instability in ionospheric plasma clouds, J. Geophys. Res., 85, 3485, 1980.

Keskinen, M.J., and S.L. Ossakow, Theories of high latitude ionospheric irregularities: A review, Radio Sci., 18, 1077, 1983.

Linson, L.M. and G. Meltz, Theory of ion cloud dynamics and morphology, in Analysis of Barium Clouds, Rep. RADC-TR-72-736, Vol. 1, chap. 5, Avco Everett Res. Lab., Everett, Mass., 1972.

Linson, L.M., and J.B. Workman, Formation of striations in ionospheric plasma clouds, J. Geophys. Res., 75, 3211, 1970.

McDonald, B.E., M.J. Keskinen, S.L. Ossakow, and S.T. Zalesak, Computer simulation of gradient drift instability processes in Operation Avefria, J. Geophys. Res., 85, 2143, 1980.

McDonald, B.E., S.L. Ossakow, S.T. Zalesak, and N.J. Zabusky, Scale sizes and lifetimes of F region plasma cloud striations as determined by the condition of marginal stability, J. Geophys. Res., 86, 5775, 1981.

Overman, E.A., N.J. Zabusky, and S.L. Ossakow, Ionospheric plasma cloud dynamics via regularized contour dynamics, I, Stability and nonlinear evolution of one-contour models, Phys. Fluids, 26, 1139, 1983.

Perkins, F.W., N.J. Zabusky, and J.H. Doles III, Deformation and striation of plasma clouds in the ionosphere, 1, J. Geophys. Res., 78, 697, 1973.

Perkins, F.W., and J.H. Doles III, Velocity shear and the $E \times B$ instability, J. Geophys. Res., 80, 211, 1975.

Prettie, C.W., U-Shaped curve constant determined by barium release measurements, Berkeley Research Assoc. Report, PD-BRA-84-320R, 1985.

Scannapieco, A.J., S.L. Ossakow, S.R. Goldman, and J.M. Pierre, Plasma cloud late time striation spectra, J. Geophys. Res., 81, 6037, 1976.

Shiau, J.N., and A. Simon, Onset of striations in barium clouds, Phys. Rev. Lett., 29, 1664, 1972.

Simon, A., Instability of a partially ionized plasma in crossed electric and magnetic fields, Phys. Fluids, 6, 382, 1963.

Smythe, W.R., Static and Dynamics Electricity, McGraw-Hill, New York, 1950, p. 65.

Sperling, J.L., Finite parallel wavelengths and ionospheric structuring, J. Geophys. Res., 88, 4075, 1983.

Sperling, J.L., The evanescence of striation parameters along the geomagnetic field, J. Geophys. Res., 89, 6793, 1984.

Sperling, J.L., J.F. Drake, S.T. Zalesak, and J.D. Huba, The role of finite parallel length on the stability of barium clouds, J. Geophys. Res., 89, 10,913, 1984.

Sperling, J.L., and A.J. Glassman, Striation eigenmodes along the geomagnetic field and eigenvalues in the limit of strong ion-neutral collisions, J. Geophys. Res., 90, 2819, 1985.

Völk, H.J., and G. Haerendel, Striations in ionospheric ion clouds, 1, J. Geophys. Res., 76, 4541, 1971.

Zabusky, N.J., J.H. Doles, III, and F.W. Perkins, Deformation and striation of plasma clouds in the ionosphere 2. Numerical simulation of a nonlinear two-dimensional model, J. Geophys. Res., 78, 711, 1973.

Zalesak, S.T., P.K. Chaturvedi, S.L. Ossakow, and J.A. Fedder, Finite temperature effects on the evolution of ionospheric barium clouds in the presence of a conducting background ionosphere, 1. The simplest case: Incompressible background ionosphere, equipotential magnetic field lines, and an altitude invariant neutral wind, J. Geophys. Res., 90, 4299, 1985.

Zalesak, S.T., and J.D. Huba, On the linear stability of two-dimensional barium clouds I. The inviscid case, NRL Memo Rept. 5312, 1984.
ADA 141284

DISTRIBUTION LIST

DEPARTMENT OF DEFENSE

ASSISTANT SECRETARY OF DEFENSE
COMM, CMD, CONT 7 INTELL
WASHINGTON, DC 20301

DIRECTOR
COMMAND CONTROL TECHNICAL CENTER
PENTAGON RM BE 685
WASHINGTON, DC 20301
  01CY ATTN C-650
  01CY ATTN C-312 R. MASON

DIRECTOR
DEFENSE ADVANCED RSCH PROJ AGENCY
ARCHITECT BUILDING
1400 WILSON BLVD.
ARLINGTON, VA 22209
  01CY ATTN NUCLEAR MONITORING RESEARCH
  01CY ATTN STRATEGIC TECH OFFICE

DEFENSE COMMUNICATION ENGINEER CENTER
1860 WIEHLE AVENUE
RESTON, VA 22090
  01CY ATTN CODE R410
  01CY ATTN CODE R812

DIRECTOR
DEFENSE NUCLEAR AGENCY
WASHINGTON, DC 20305
  01CY ATTN STVL
  04CY ATTN TITL
  01CY ATTN DDST
  03CY ATTN RAAE

COMMANDER
FIELD COMMAND
DEFENSE NUCLEAR AGENCY
KIRTLAND, AFB, NM 87115
  01CY ATTN FCPR

DEFENSE NUCLEAR AGENCY
SAO/DNA
BUILDING 20676
KIRTLAND AFB, NM 87115
  01CY D.C. THORNBURG

DIRECTOR
INTERSERVICE NUCLEAR WEAPONS SCHOOL
KIRTLAND AFB, NM 87115
  01CY ATTN DOCUMENT CONTROL

JOINT PROGRAM MANAGEMENT OFFICE
WASHINGTON, DC 20330
  01CY ATTN J-3 WWMCCS EVALUATION OFFICE

DIRECTOR
JOINT STRAT TGT PLANNING STAFF
OFFUTT AFB
OMAHA, NB 68113
  01CY ATTN JSTPS/JLKS
  01CY ATTN JPST G. GOETZ

CHIEF
LIVERMORE DIVISION FLD COMMAND DNA
DEPARTMENT OF DEFENSE
LAWRENCE LIVERMORE LABORATORY
P.O. BOX 808
LIVERMORE, CA 94550
  01CY ATTN FCPRL

COMMANDANT
NATO SCHOOL (SHAPE)
APO NEW YORK 09172
  01CY ATTN U.S. DOCUMENTS OFFICER

UNDER SECY OF DEF FOR RSCH & ENGRG
DEPARTMENT OF DEFENSE
WASHINGTON, DC 20301
  01CY ATTN STRATEGIC & SPACE SYSTEMS (OS)

COMMANDER/DIRECTOR
ATMOSPHERIC SCIENCES LABORATORY
U.S. ARMY ELECTRONICS COMMAND
WHITE SANDS MISSILE RANGE, NM 88002
  01CY ATTN DELAS-EO, F. NILES

DIRECTOR
BMD ADVANCED TECH CTR
HUNTSVILLE OFFICE
P.O. BOX 1500
HUNTSVILLE, AL 35807
  01CY ATTN ATC-T MELVIN T. CAPPS
  01CY ATTN ATC-O W. DAVIES
  01CY ATTN ATC-R DON RUSS

PROGRAM MANAGER
BMD PROGRAM OFFICE
5001 EISENHOWER AVENUE
ALEXANDRIA, VA 22333
  01CY ATTN DACS-BMT J. SHEA

CHIEF C-E- SERVICES DIVISION
U.S. ARMY COMMUNICATIONS CMD
PENTAGON RM 1B269
WASHINGTON, DC 20310
  01CY ATTN C- E-SERVICES DIVISION

COMMANDER
FRADCOM TECHNICAL SUPPORT ACTIVITY
DEPARTMENT OF THE ARMY
FORT MONMOUTH, N.J. 07703
  01CY ATTN DRSEL-NL-RD H. BENNET
  01CY ATTN DRSEL-PL-ENV H. BOMKE
  01CY ATTN J.E. QUIGLEY

COMMANDER
U.S. ARMY COMM-ELEC ENGRG INSTAL AGY
FT. HUACHUCA, AZ 85613
  01CY ATTN CCC-EMEO GEORGE LANE

COMMANDER
U.S. ARMY FOREIGN SCIENCE & TECH CTR
220 7TH STREET, NE
CHARLOTTESVILLE, VA 22901
  01CY ATTN DRXST-SD

COMMANDER
U.S. ARMY MATERIAL DEV & READINESS CMD
5001 EISENHOWER AVENUE
ALEXANDRIA, VA 22333
  01CY ATTN DRCLDC J.A. BENDER

COMMANDER
U.S. ARMY NUCLEAR AND CHEMICAL AGENCY
7500 BACKLICK ROAD
BLDG 2073
SPRINGFIELD, VA 22150
  01CY ATTN LIBRARY

DIRECTOR
U.S. ARMY BALLISTIC RESEARCH
LABORATORY
ABERDEEN PROVING GROUND, MD 21005
  01CY ATTN TECH LIBRARY,
  EDWARD BAICY

COMMANDER
U.S. ARMY SATCOM AGENCY
FT. MONMOUTH, NJ 07703
  01CY ATTN DOCUMENT CONTROL

COMMANDER
U.S. ARMY MISSILE INTELLIGENCE AGENCY
REDSTONE ARSENAL, AL 35809
  01CY ATTN JIM GAMBLE

DIRECTOR
U.S. ARMY TRADOC SYSTEMS ANALYSIS
ACTIVITY
WHITE SANDS MISSILE RANGE, NM 88002
  01CY ATTN ATAA-SA
  01CY ATTN TCC/F. PAYAN JR.
  01CY ATTN ATTA-TAC LTC J. HESSE

COMMANDER
NAVAL ELECTRONIC SYSTEMS COMMAND
WASHINGTON, DC 20360
  01CY ATTN NAVALEX 034 T. HUGHES
  01CY ATTN PME 117
  01CY ATTN PME 117-T
  01CY ATTN CODE 5011

COMMANDING OFFICER
NAVAL INTELLIGENCE SUPPORT CTR
4301 SUITLAND ROAD, BLDG. 5
WASHINGTON, DC 20390
  01CY ATTN MR. DUBBIN STIC 12
  01CY ATTN NISC-50
  01CY ATTN CODE 5404 J. GALET

COMMANDER
NAVAL OCCEAN SYSTEMS CENTER
SAN DIEGO, CA 92152
  01CY ATTN J. FERGUSON

NAVAL RESEARCH LABORATORY
WASHINGTON, DC 20375
  01CY ATTN CODE 4700 S.L. Ossakow,
    26 CYS IF UNCLASS
    (01CY IF CLASS)
    ATTN CODE 4780 J.D. HUBA, 50
    CYS IF UNCLASS, 01CY IF CLASS
  01CY ATTN CODE 4701 I. VITKOVITSKY
  01CY ATTN CODE 7500
  01CY ATTN CODE 7550
  01CY ATTN CODE 7580
  01CY ATTN CODE 7551
  01CY ATTN CODE 7555
  01CY ATTN CODE 4730 E. MCLEAN
  01CY ATTN CODE 4108
  01CY ATTN CODE 4730 B. RIPIN
  20CY ATTN CODE 2628

COMMANDER
NAVAL SPACE SURVEILLANCE SYSTEM
DAHLGREN, VA 22448
  01CY ATTN CAPT J.H. BURTON

OFFICER-IN-CHARGE
NAVAL SURFACE WEAPONS CENTER
WHITE OAK, SILVER SPRING, MD 20910
  01CY ATTN CODE F31

DIRECTOR
STRATEGIC SYSTEMS PROJECT OFFICE
DEPARTMENT OF THE NAVY
WASHINGTON, DC 20376
  01CY ATTN NSP-2141
  01CY ATTN NSSP-2722 FRED WIMBERLY

COMMANDER
NAVAL SURFACE WEAPONS CENTER
DAHLGREN LABORATORY
DAHLGREN, VA 22448
  01CY ATTN CODE DF-14 R. BUTLER

OFFICER OF NAVAL RESEARCH
ARLINGTON, VA 22217
  01CY ATTN CODE 465
  01CY ATTN CODE 461
  01CY ATTN CODE 402
  01CY ATTN CODE 420
  01CY ATTN CODE 421

COMMANDER
AEROSPACE DEFENSE COMMAND/DC
DEPARTMENT OF THE AIR FORCE
ENT AFB, CO 80912
  01CY ATTN DC MR. LONG

COMMANDER
AEROSPACE DEFENSE COMMAND/XPD
DEPARTMENT OF THE AIR FORCE
ENT AFB, CO 80912
  01CY ATTN XPDQQ
  01CY ATTN XP

AIR FORCE GEOPHYSICS LABORATORY
HANSCOM AFB, MA 01731
  01CY ATTN OPR HAROLD GARDNER
  01CY ATTN LKB
    KENNETH S.W. CHAMPION
  01CY ATTN OPR ALVA T. STAIR
  01CY ATTN PHD JURGEN BUCHAU
  01CY ATTN PHD JOHN P. MULLEN

AF WEAPONS LABORATORY
KIRTLAND AFT, NM 87117
  01CY ATTN SUL
  01CY ATTN CA ARTHUR H. GUENTHER
  01CY ATTN NTYCE 1LT. G. KRAJEI

AFTAC
PATRICK AFB, FL 32925
  01CY ATTN TN

AIR FORCE AVIONICS LABORATORY
WRIGHT-PATTERSON AFB, OH 45433
  01CY ATTN AAD WADE HUNT
  01CY ATTN AAD ALLEN JOHNSON

DEPUTY CHIEF OF STAFF
RESEARCH, DEVELOPMENT, & ACQ.
DEPARTMENT OF THE AIR FORCE
WASHINGTON, DC 20330
  01CY ATTN AFRDQ

HEADQUARTERS
ELECTRONIC SYSTEMS DIVISION
DEPARTMENT OF THE AIR FORCE
HANSCOM AFB, MA 01731-5000
  01CY ATTN J. DEAS
    ESD/SCD-4

COMMANDER
FOREIGN TECHNOLOGY DIVISION, AFSC
WRIGHT-PATTERSON AFB, OH 45433
01CY ATTN NICD LIBRARY
01CY ATTN ETDP B. BALLARD

COMMANDER
ROME AIR DEVELOPMENT CENTER, AFSC
GRIFFISS AFB, NY 13441
01CY ATTN DOC LIBRARY/TSLD
01CY ATTN OCSE V. COYNE

STRATEGIC AIR COMMAND/XPFS
OFFUTT AFB, NB 68113
01CY ATTN ADWATE MAJ BRUCE BAUER
01CY ATTN NRT
01CY ATTN DOK CHIEF SCIENTIST

SAMSO/SK
P.O. BOX 92960
WORLDWAY POSTAL CENTER
LOS ANGELES, CA 90009
01CY ATTN SKA (SPACE COMM SYSTEMS) M. CLAVIN

SAMSO/MN
NORTON AFB, CA 92409
(MINUTEMAN)
01CY ATTN MNNL

COMMANDER
ROME AIR DEVELOPMENT CENTER, AFSC
HANSCOM AFB, MA 01731
01CY ATTN EEP A. LORENTZEN

DEPARTMENT OF ENERGY
LIBRARY ROOM G-042
WASHINGTON, DC 20545
01CY ATTN DOC CON FOR A. LABOWITZ

DEPARTMENT OF ENERGY
ALBUQUERQUE OPERATIONS OFFICE
P.O. BOX 5400
ALBUQUERQUE, NM 87115
01CY ATTN DOC CON FOR D. SHERWOOD

EG&G, INC.
LOS ALAMOS DIVISION
P.O. BOX 809
LOS ALAMOS, NM 85544
01CY ATTN DOC CON FOR J. BREEDLOVE

UNIVERSITY OF CALIFORNIA
LAWRENCE LIVERMORE LABORATORY
P.O. BOX 808
LIVERMORE, CA 94550
01CY ATTN DOC CON FOR TECH INFO DEPT
01CY ATTN DOC CON FOR L-389 R. OTT
01CY ATTN DOC CON FOR L-31 R. HAGEI

LOS ALAMOS NATIONAL LABORATORY
P.O. BOX 1663
LOS ALAMOS, NM 87545
01CY ATTN DOC CON FOR J. WOLCOTT
01CY ATTN DOC CON FOR R.F. TASCHEK
01CY ATTN DOC CON FOR E. JONES
01CY ATTN DOC CON FOR J. MALIK
01CY ATTN DOC CON FOR R. JEFFRIES
01CY ATTN DOC CON FOR J. ZINN
01CY ATTN DOC CON FOR D. WESTERVEL
01CY ATTN D. SAPPENFIELD

LOS ALAMOS NATIONAL LABORATORY
MS D438
LOS ALAMOS, NM 87545
01CY ATTN S.P. GARY
01CY ATTN J. BOROVSKY

SANDIA LABORATORIES
P.O. BOX 5800
ALBUQUERQUE, NM 87115
01CY ATTN DOC CON FOR W. BROWN
01CY ATTN DOC CON FOR A. THORNBROUGH
01CY ATTN DOC CON FOR T. WRIGHT
01CY ATTN DOC CON FOR D. DAHLGREN
01CY ATTN DOC CON FOR 3141
01CY ATTN DOC CON FOR SPACE PROJEC DIV

SANDIA LABORATORIES
LIVERMORE LABORATORY
P.O. BOX 969
LIVERMORE, CA 94550
01CY ATTN DOC CON FOR B. MURPHEY
01CY ATTN DOC CON FOR T. COOK

OFFICE OF MILITARY APPLICATION
DEPARTMENT OF ENERGY
WASHINGTON, DC 20545
01CY ATTN DOC CON DR. YO SONG

OTHER GOVERNMENT

INSTITUTE FOR TELECOM SCIENCES
NATIONAL TELECOMMUNICATIONS & INFO
ADMIN
BOULDER, CO 80303
01CY ATTN D. CROMBIE
01CY ATTN L. BERRY

NATIONAL OCEANIC & ATMOSPHERIC ADMIN
ENVIRONMENTAL RESEARCH LABORATORIES
DEPARTMENT OF COMMERCE
BOULDER, CO 80302
01CY ATTN R. GRUBB
01CY ATTN AERONOMY LAB G. REID

DEPARTMENT OF DEFENSE CONTRACTORS

AEROSPACE CORPORATION
P.O. BOX 92957
LOS ANGELES, CA 90009
01CY ATTN I. GARFUNKEL
01CY ATTN T. SALMI
01CY ATTN V. JOSEPHSON
01CY ATTN S. BOWER
01CY ATTN D. OLSEN

ANALYTICAL SYSTEMS ENGINEERING CORP
5 OLD CONCORD ROAD
BURLINGTON, MA 01803
01CY ATTN RADIO SCIENCES

AUSTIN RESEARCH ASSOC., INC.
1901 RUTLAND DRIVE
AUSTIN, TX 78758
01CY ATTN L. SLOAN
01CY ATTN R. THOMPSON

BERKELEY RESEARCH ASSOCIATES, INC.
P.O. BOX 983
BERKELEY, CA 94701
01CY ATTN J. WORKMAN
01CY ATTN C. PRETTIE
01CY ATTN S. BRECHT

BOEING COMPANY, THE
P.O. BOX 3707
SEATTLE, WA 98124
01CY ATTN G. KEISTER
01CY ATTN D. MURRAY
01CY ATTN G. HALL
01CY ATTN J. KENNEY

CHARLES STARK DRAPER LABORATORY, INC.
555 TECHNOLOGY SQUARE
CAMBRIDGE, MA 02139
01CY ATTN D.B. COX
01CY ATTN J.P. GILMORE

COMSAT LABORATORIES
LINTHICUM ROAD
CLARKSBURG, MD 20734
01CY ATTN G. HYDE

CORNELL UNIVERSITY
DEPARTMENT OF ELECTRICAL ENGINEERING
ITHACA, NY 14850
01CY ATTN D.T. FARLEY, JR.

ELECTROSPACE SYSTEMS, INC.
BOX 1359
RICHARDSON, TX 75080
01CY ATTN H. LOGSTON
01CY ATTN SECURITY (PAUL PHILLIPS)

EOS TECHNOLOGIES, INC.
606 Wilshire Blvd.
Santa Monica, CA 90401
01CY ATTN C.B. GABBARD
01CY ATTN R. LELEVIER

ESL, INC.
495 JAVA DRIVE
SUNNYVALE, CA 94086
01CY ATTN J. ROBERTS
01CY ATTN JAMES MARSHALL

GENERAL ELECTRIC COMPANY
SPACE DIVISION
VALLEY FORGE SPACE CENTER
GODDARD BLVD KING OF PRUSSIA
P.O. BOX 8555
PHILADELPHIA, PA 19101
01CY ATTN M.H. BORTNER
SPACE SCI LAB

GENERAL ELECTRIC TECH SERVICES
CO., INC.
HMES
COURT STREET
SYRACUSE, NY 13201
01CY ATTN G. MILLMAN

GEOPHYSICAL INSTITUTE
UNIVERSITY OF ALASKA
FAIRBANKS, AK 99701
(ALL CLASS ATTN: SECURITY OFFICER)
01CY ATTN T.N. DAVIS (UNCLASS ONLY)
01CY ATTN TECHNICAL LIBRARY
01CY ATTN NEAL BROWN (UNCLASS ONLY)

GTE SYLVANIA, INC.
ELECTRONICS SYSTEMS GRP-EASTERN DIV
77 A STREET
NEEDHAM, MA 02194
01CY ATTN DICK STEINHOF

HSS, INC.
2 ALFRED CIRCLE
BEDFORD, MA 01730
01CY ATTN DONALD HANSEN

ILLINOIS, UNIVERSITY OF
107 COBLE HALL
150 DAVENPORT HOUSE
CHAMPAIGN, IL 61820
(ALL CORRES ATTN DAN MCCLELLAND)
01CY ATTN K. YEH

INSTITUTE FOR DEFENSE ANALYSES
1801 NO. BEAUREGARD STREET
ALEXANDRIA, VA 22311
01CY ATTN J.M. AEIN
01CY ATTN ERNEST BAUER
01CY ATTN HANS WOLFARD
01CY ATTN JOEL BENGSTON

INTL TEL & TELEGRAPH CORPORATION
500 WASHINGTON AVENUE
NUTLEY, NJ 07110
01CY ATTN TECHNICAL LIBRARY

JAYCOR
11011 TORREYANA ROAD
P.O. BOX 85154
SAN DIEGO, CA 92138
01CY ATTN J.L. SPERLING

JOHNS HOPKINS UNIVERSITY
APPLIED PHYSICS LABORATORY
JOHNS HOPKINS ROAD
LAUREL, MD 20810
01CY ATTN DOCUMENT LIBRARIAN
01CY ATTN THOMAS POTEMRA
01CY ATTN JOHN DASSOULAS

KAMAN SCIENCES CORP
P.O. BOX 7463
COLORADO SPRINGS, CO 80933
01CY ATTN T. MEAGHER

KAMAN TEMPO-CENTER FOR ADVANCED STUDIES
816 STATE STREET (P.O DRAWER QQ)
SANTA BARBARA, CA 93102
01CY ATTN DASIAC
01CY ATTN WARREN S. KNAPP
01CY ATTN WILLIAM MCNAMARA
01CY ATTN B. GAMBILL

LINKABIT CORP
10453 ROSELLE
SAN DIEGO, CA 92121
01CY ATTN IRWIN JACOBS

LOCKHEED MISSILES & SPACE CO., INC
P.O. BOX 504
SUNNYVALE, CA 94088
01CY ATTN DEPT 60-12
01CY ATTN D.R. CHURCHILL

LOCKHEED MISSILES & SPACE CO., INC.
3251 HANOVER STREET
PALO ALTO, CA 94304
01CY ATTN MARTIN WALT DEPT 52-12
01CY ATTN W.L. IMHOF DEPT 52-12
01CY ATTN RICHARD G. JOHNSON DEPT 52-12
01CY ATTN J.B. CLADIS DEPT 52-12

MARTIN MARIETTA CORP
ORLANDO DIVISION
P.O. BOX 5837
ORLANDO, FL 32805
01CY ATTN R. HEFFNER

MCDONNEL DOUGLAS CORPORATION
5301 BOLSA AVENUE
HUNTINGTON BEACH, CA 92647
01CY ATTN N. HARRIS
01CY ATTN J. MOULE
01CY ATTN GEORGE MROZ
01CY ATTN W. OLSON
01CY ATTN R.W. HALPRIN
01CY ATTN TECHNICAL LIBRARY SERVICES

MISSION RESEARCH CORPORATION
735 STATE STREET
SANTA BARBARA, CA 93101
  01CY ATTN P. FISCHER
  01CY ATTN W.F. CREVIER
  01CY ATTN STEVEN L. GUTSCHE
  01CY ATTN R. BOGUSCH
  01CY ATTN R. HENDRICK
  01CY ATTN RALPH KILB
  01CY ATTN DAVE SOWLE
  01CY ATTN F. FAJEN
  01CY ATTN M. SCHEIBE
  01CY ATTN CONRAD L. LONGMIRE
  01CY ATTN B. WHITE
  01CY ATTN R. STAGAT

MISSION RESEARCH CORP.
1720 RANDOLPH ROAD, S.E.
ALBUQUERQUE, NM 87106
  01CY R. STELLINGWERF
  01CY M. ALME
  01CY L. WRIGHT

MITRE CORP
WESTGATE RESEARCH PARK
1820 DOLLY MADISON BLVD
MCLEAN, VA 22101
  01CY ATTN W. HALL
  01CY ATTN W. FOSTER

PACIFIC-SIERRA RESEARCH CORP
12340 SANTA MONICA BLVD.
LOS ANGELES, CA 90025
  01CY ATTN E.C. FIELD, JR.

PENNSYLVANIA STATE UNIVERSITY
IONOSPHERE RESEARCH LAB
318 ELECTRICAL ENGINEERING EAST
UNIVERSITY PARK, PA 16802
  (NO CLASS TO THIS ADDRESS)
  01CY ATTN IONOSPHERIC RESEARCH LAB

PHOTOMETRICS, INC.
4 ARROW DRIVE
WOBURN, MA 01801
  01CY ATTN IRVING L. KOFSKY

PHYSICAL DYNAMICS, INC.
P.O. BOX 3027
BELLEVUE, WA 98009
  01CY ATTN E.J. FREMOUW

PHYSICAL DYNAMICS, INC.
P.O. BOX 10367
OAKLAND, CA 94610
  ATTN A. THOMSON

R & D ASSOCIATES
P.O. BOX 9695
MARINA DEL REY, CA 90291
  01CY ATTN FORREST GILMORE
  01CY ATTN WILLIAM B. WRIGHT, JR.
  01CY ATTN WILLIAM J. KARZAS
  01CY ATTN H. ORY
  01CY ATTN C. MACDONALD

RAND CORPORATION, THE
15450 COHASSET STREET
VAN NUYS, CA 91406
  01CY ATTN CULLEN CRAIN
  01CY ATTN ED BEDROZIAN

RAYTHEON CO.
528 BOSTON POST ROAD
SUDBURY, MA 01776
  01CY ATTN BARBARA ADAMS

RIVERSIDE RESEARCH INSTITUTE
330 WEST 42nd STREET
NEW YORK, NY 10036
  01CY ATTN VINCE TRAPANI

SCIENCE APPLICATIONS, INC.
1150 PROSPECT PLAZA
LA JOLLA, CA 92037
  01CY ATTN LEWIS M. LINSON
  01CY ATTN DANIEL A. HAMLIN
  01CY ATTN E. FRIEMAN
  01CY ATTN E.A. STRAKER
  01CY ATTN CURTIS A. SMITH

SCIENCE APPLICATIONS, INC
1710 GOODRIDGE DR.
MCLEAN, VA 22102
  01CY J. COCKAYNE
  01CY E. HYMAN

SRI INTERNATIONAL
333 RAVENSWOOD AVENUE
MENLO PARK, CA 94025
01CY ATTN J. CASPER
01CY ATTN DONALD NEILSON
01CY ATTN ALAN BURNS
01CY ATTN G. SMITH
01CY ATTN R. TSUNODA
01CY ATTN DAVID A. JOHNSON
01CY ATTN WALTER G. CHESNUT
01CY ATTN CHARLES L. RINO
01CY ATTN WALTER JAYE
01CY ATTN J. VICKREY
01CY ATTN RAY L. LEADABRAND
01CY ATTN G. CARPENTER
01CY ATTN G. PRICE
01CY ATTN R. LIVINGSTON
01CY ATTN V. GONZALES
01CY ATTN D. MCDANIEL

TECHNOLOGY INTERNATIONAL CORP
75 WIGGINS AVENUE
BEDFORD, MA 01730
01CY ATTN W.P. BOQUIST

TRW DEFENSE & SPACE SYS GROUP
ONE SPACE PARK
REDONDO BEACH, CA 90278
01CY ATTN R. K. PLEBUCH
01CY ATTN S. ALTSCHULER
01CY ATTN D. DEE
01CY ATTN D/ STOCKWELL
SNTF/1575

VISIDYNE
SOUTH BEDFORD STREET
BURLINGTON, MA 01803
01CY ATTN W. REIDY
01CY ATTN J. CARPENTER
01CY ATTN C. HUMPHREY

UNIVERSITY OF PITTSBURGH
PITTSBURGH, PA 15213
01CY ATTN: N. ZABUSKY

DTIC
02CY

CODE 1220
01CY

DIRECTOR OF RESEARCH
U.S. NAVAL ACADEMY
ANNAPOLIS, MD 21402
02CY

END

FILMED

5-86

DTIC